# Observation of Nondipole-Induced Asymmetry in the Angular Emission Distribution of Photoelectrons from Fixed-in-Space CO Molecules

D. V. Rezvan,[1] K. Klyssek,[2] S. Grundmann,[2] A. Pier,[2] N. M. Novikovskiy,[1] N. Strenger,[2] D. Tsitsonis,[2] M. Kircher,[2] I. Vela-Peréz,[2] K. Fehre,[2] F. Trinter,[3,4] M. S. Schöffler,[2] T. Jahnke,[5] R. Dörner,[2,*] and Ph. V. Demekhin[1,†]

[1]*Institut für Physik und CINSaT, Universität Kassel, Heinrich-Plett-Straße 40, 34132 Kassel, Germany*
[2]*Institut für Kernphysik, J. W. Goethe-Universität, Max-von-Laue-Straße 1, 60438 Frankfurt am Main, Germany*
[3]*FS-PETRA-S, Deutsches Elektronen-Synchrotron (DESY), Notkestraße 85, 22607 Hamburg, Germany*
[4]*Molecular Physics, Fritz-Haber-Institut der Max-Planck-Gesellschaft, Faradayweg 4-6, 14195 Berlin, Germany*
[5]*European XFEL GmbH, Holzkoppel 4, 22869 Schenefeld, Germany*

(Received 10 August 2022; revised 1 November 2022; accepted 4 November 2022; published 14 December 2022)

We investigate experimentally and theoretically the C and O 1*s* photoionization of fixed-in-space CO molecules at a photon energy of 905 eV. We find a significant dependence of the photoelectron angular distributions on the direction of propagation of the ionizing radiation. It results from an interplay of nondipole effects, on one hand, and molecular effects, on the other. The nondipole effects lead to an increase of the emission probability in the forward direction along the light propagation, and the photoelectron wave being scattered by the molecular potential gives rise to a strong peak in the direction of the atom neighboring the emitter site. These effects can either conspire or extenuate each other, depending on the photoelectron emission direction and molecular orientation in space.

DOI: 10.1103/PhysRevLett.129.253201

Over a wide range of wavelengths and intensities, light-driven electron emission does mainly depend on the light's polarization but only weakly on its propagation direction. This is the rationale for the electric-dipole approximation used in many theoretical treatments. That approximation entails the neglect of the photon momentum, the finite speed of light, and the spatial dependence as well as the magnetic component of the electromagnetic wave. Refined experimental precision, however, has lead to the observation of the imprints of all of these effects in, e.g., the photoelectron momentum (angular emission) [1–3] distributions and even the photoelectron energy [4]. Starting about 10 years ago, ever more sensitive experiments in strong-field multiphoton processes uncovered many intriguing details, e.g., on the forward shift of the momentum distribution by magnetic [5–8] as well as electric [9] nondipole effects, and found that the energy of the photoelectron peaks changes with the emission direction relatively to the light propagation [4]. In the perturbative regime of single-photon ionization, furthermore, the role of the photon momentum on the photoelectric effect was directly shown in experiments by Grundmann *et al.* [10], the finite speed of light was shown to induce zeptosecond delays in the birth time of the photoelectron wave [11], and a long illusive dipole-forbidden mechanism for double ionization was proposed [12] and experimentally confirmed several years later [13,14].

These studies examined the nondipole contributions emerging due to the nature of light itself. As these experiments mainly investigated atoms (or randomly oriented molecules) as targets, they mostly neglected the influence of the geometrical properties of those targets. In molecular photoionization, the interaction of the emitted photoelectrons with the multicenter molecular potential plays a dominant role, as is shown, for example, in cases where molecular-frame photoelectron angular distributions [15–17] are employed even as a tool for structure determination. Despite at high photon energies both of these two building blocks are naturally shaping the photoelectron emission process, they have rarely been looked at jointly (see Ref. [18] for pioneering work which made use of a powerful experimental setup of Ref. [19]). It is the purpose of the present Letter to show on the example of single-photon *K*-shell ionization of CO how the molecular effects and the nondipole effects finally determine the outcome of the photoionization process. While the molecular effects decrease with photon energy (as fast photoelectrons are less affected by the molecular potential), on the contrary, nondipole effects increase with photon energy. We, therefore, chose a photon energy of $h\nu = 905$ eV, where both effects can be expected to be appreciably strong.

In almost all atomic and molecular photoionization studies, the nondipole contributions manifest themselves

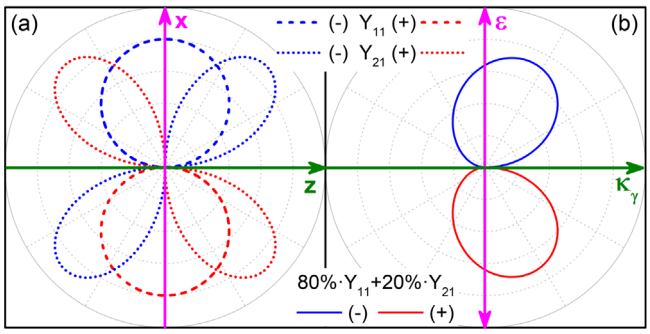


FIG. 1. (a) Normalized dipole ($Y_{11}$, dashed curves) and quadrupole ($Y_{21}$, dotted curves) amplitudes in the $xz$ plane. Red represents positive and blue negative signs. The phase difference between those amplitudes changes stepwise by $\pi$ going from the forward to the backward emission directions. (b) 80%:20% mixture of the dipole and quadrupole amplitudes, which is bent to the forward direction of the propagation $k_\gamma$ of circularly polarized light.

via a forward-backward asymmetry of the angular emission distributions of photoelectrons in the laboratory frame [2,3,20]. A simplified physical picture behind this effect can be demonstrated with the help of Fig. 1. Let us consider the $K$-shell ionization of an atom with circularly polarized light of positive helicity which propagates along the $z$ axis. In the electric-dipole approximation, it emits an $\epsilon p$ wave with an amplitude for its momentum distribution as given by the $Y_{11}$ spherical function [dashed curve in Fig. 1(a)]. The quadrupole interaction populates an $\epsilon d$ wave whose momentum-distribution amplitude is given by the $Y_{21}$ function [dotted curve in Fig. 1(a); compare Fig. 1 in Ref. [14] for experimental demonstration]. As one can see, the dipole and quadrupole contributions possess similar signs for $z > 0$ and opposite signs for $z < 0$ (as encoded in their colors). As a consequence, a superposition of those contributions results in an angular emission distribution with considerably more electrons being emitted along the light propagation direction $\mathbf{k}_\gamma$, i.e., in the forward direction [see the solid curve in Fig. 1(b) representing a 80%:20% mixture of the amplitudes].

One can expect that this simple physical picture changes considerably for molecules. First, owing to the loss of central symmetry, the photoelectron can exchange angular momentum with the molecular ion. Thus, many partial photoelectron waves mix in the dipole and also in all multipole contributions, and a more complicated dependence of the phase difference between those contributions (and of their superposition) on the emission angle can be expected (even for randomly oriented molecules). Second, the nondipole contributions can be expected to be different for different molecular orientations, depending on the spatial configuration of scattering neighbor atoms. Indeed, a variety of asymmetries in photoelectron angular distributions from fixed-in-space molecules and in the laboratory-frame angular distributions of fragments, emerging beyond the electric-dipole approximation, was predicted analytically almost 20 years ago [21]. Here, we investigate experimentally and theoretically one of such nondipole-induced asymmetries.

The interplay of nondipole effects and molecular multiple scattering is illustrated with the help of our theoretical results in Fig. 2. This figure depicts the angular emission distribution of the carbon and oxygen $1s$ photoelectrons of a CO molecule, computed in different approximations. The molecule lies in the picture plane and is oriented such that the carbon atom points toward $+45°$ and $-45°$ with respect to the polarization plane $\epsilon$ of the circularly polarized light (i.e., in the forward and backward directions with respect to the light propagation axis $k_\gamma$). The calculations were carried out in the frozen-core Hartree-Fock approximation using the stationary single center (SC) method [22–24], which allows for an accurate description of angle-resolved molecular photoionization. In the calculations, molecular orbitals of the bound electrons of the neutral CO molecule were generated at the equilibrium internuclear distance of 2.132 a.u. [25] using the PC GAMESS (U.S.) [26] QC package in the triplet-zeta valence basis set [27]. They were further decomposed over the spherical functions with $\ell < 99$ and $m = 0$ or $m = \pm 1$ (for $\sigma$ or $\pi$ orbitals, respectively) with respect to the geometrical center of the molecule and used to generate the electrostatic direct and exchange Coulomb potentials for the photoelectron. In order to properly describe the underlying nondipole effects, angular-momentum quantum numbers $\ell < 50$ and $m < 5$ were included in the calculations of the partial photoelectron waves with the kinetic energies of 609 and 363 eV, respectively, for the C and O $1s$ ionizations. The photoionization amplitudes for emission of partial photoelectron waves were computed in the velocity gauge by treating the plane wave $e^{i\mathbf{k}_\gamma \cdot \mathbf{r}}$ of the vector potential in the transition matrix element explicitly and performing a three-dimensional integration in the molecular frame numerically [28].

As one can see from Fig. 2, the computed angular emission distributions exhibit the strong main lobe in the direction of the scatterer, showing the ability of high-energy photoelectrons to image a neighboring atom [29,30]. It emerges because a photoelectron wave emitted toward a heavy neighbor is attracted by an uncompensated positive charge of its nucleus, which focuses it as a lens. In the dipole approximation with $e^{i\mathbf{k}_\gamma \cdot \mathbf{r}} \approx 1$ (dashed blue curves), the two emission patterns computed for $+45°$ and $-45°$ orientations of the molecule are perfect mirror images of each other with respect to the polarization plane (vertical magenta double arrow). If the plane wave $e^{i\mathbf{k}_\gamma \cdot \mathbf{r}}$ is fully included in the calculations (solid black curve), the underlying nondipole effects cause a systematic enhancement and reduction of the angular distributions, respectively, in the forward and backward emission directions with respect to the propagation of the light. As a consequence, the main lobe in the computed distributions is larger if the scatterer

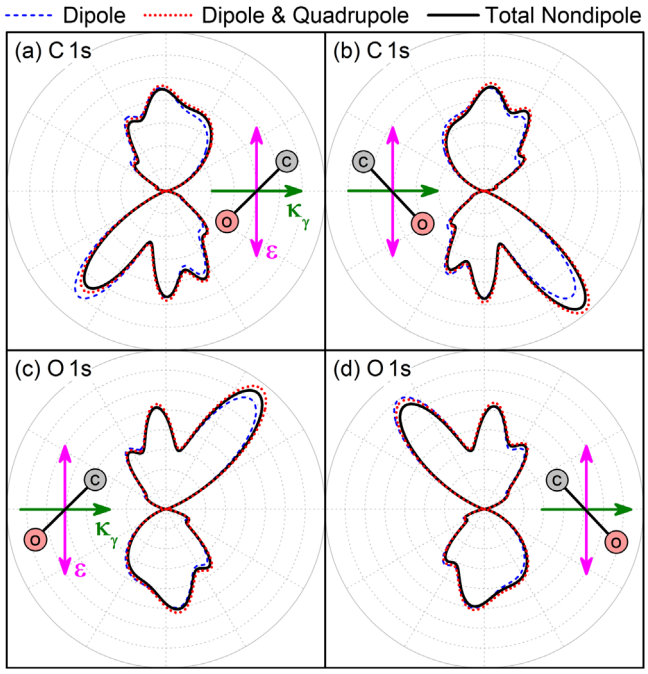


FIG. 2. Angular emission distributions of 1$s$ photoelectrons after ionization of CO molecules by photons with an energy of 905 eV, as computed in different approximations. (a) and (b) Carbon 1$s$ photoelectrons. (c) and (d) Oxygen 1$s$ photoelectrons. Light propagates horizontally from left to right (green arrow). The molecule is oriented in the picture plane at $+45°$ in (a) and (c) and at $-45°$ in (b) and (d) with respect to the polarization plane (which is perpendicular to the picture plane, indicated by magenta double arrow) of the circularly polarized light. The photoelectrons are emitted in the plane built by the light propagation and molecular orientation axes. Dashed blue curve, dipole approximation. Dotted red curve, dipole and quadrupole contributions. Solid black curve, full nondipole treatment.

points in the forward direction, creating a notable asymmetry of the emission patterns for the two selected molecular orientations. Additional calculations performed approximating $e^{i\mathbf{k}_\gamma\cdot\mathbf{r}} \approx 1 + i\mathbf{k}_\gamma \cdot \mathbf{r}$ (dotted red curves) suggest that the quadrupole contribution underestimates the full effect in the backward emission direction and overestimates it in the forward direction.

In order to verify this nondipole-induced asymmetry, we performed an experiment at the soft x-ray beam line P04 of the synchrotron PETRA III [31] at DESY in Hamburg (Germany) in few-bunch timing mode (bunch spacing 192 ns). A supersonic CO molecular beam was crossed with the circularly polarized synchrotron radiation provided by the 5-m-long APPLE-II undulator at the photon energy of 905 eV. All charged particles generated in the course of the photoionization, Auger decay, and subsequent Coulomb explosion of the molecule were detected in coincidence by using the COLTRIMS (cold target recoil ion momentum spectroscopy) reaction microscope [32–34] permanently installed at the beam line. Electrons and ions were guided by homogeneous electric (56.1 V/cm) and magnetic (43.5 G) fields in two opposite arms onto two time- and position-sensitive microchannel plate (MCP) detectors (active area of 80 mm diameter) with hexagonal delay-line position readout [35,36]. The employed electron arm was in total 166 mm long and included an additional mesh for creating a drift region (time-of-flight focusing geometry). The employed ion arm was in total 308 mm long and included an electrostatic lens (time-of-flight and spatial focusing) plus spectrometer plates of smaller inner diameter to shield the target region from this electrostatic lens. The electron arm of the spectrometer allowed for an efficient detection of high-energy C and O 1$s$ photoelectrons and subsequent Auger electrons.

The initial momentum vectors of charged particles can be determined from their positions of impact on the detectors and their flight times. Under assumption of the axial-recoil approximation [37], the ionic momenta provide access to the molecular orientation at the instant of photoionization. The photoelectron momenta measured in coincidence yield in addition the relative emission angles. The measured angular emission distributions of the C and O 1$s$ photoelectrons are depicted, respectively, in Figs. 3 and 4 for selected orientations of the molecule with respect to the polarization plane. They are compared to the respective theoretical distribution. The error bars represent the absolute statistical uncertainties of the measured data (i.e., the square root of the number of counts). As one can see from these figures, the experimental results are in good agreement with the computed ones, confirming thereby the predicted nondipole-induced asymmetry. In particular, the emission distributions obtained for two mirrored orientations of the molecule with respect to the polarization plane, i.e., for the $\pm\alpha$ angles, are not perfect mirror images of each other as they would be within the dipole approximation. Indeed, both theory and experiment exhibit a clearly larger main lobe if the scatterer atom points in the forward direction (negative orientation angles in Fig. 3 and positive in Fig. 4) as compared to the cases where the neighbor points backward with respect to the light propagation (for $+\alpha$ orientations in Fig. 3 and for $-\alpha$ in Fig. 4).

Although many details in the theoretical emission distributions are reproduced by the experiment, there is a quantitative disagreement between the measurement and the prediction which can be rationalized as follows. First, the measured data represent photoelectrons emitted within an opening angle of $\pm 12°$ out of the plane which is spanned by the molecular axis and the light propagation direction (the picture plane). In order to demonstrate the largest nondipole-induced asymmetry, the computed data are restricted to this plane only. Extended calculations, however, indicated a small impact of the close-lying out-of-plane emission directions on the effect. Second, the photoelectron emission angles are binned in steps of 6°. Finally and most importantly, in order to gather sufficient statistics, the experimental data are gated on intervals for molecular

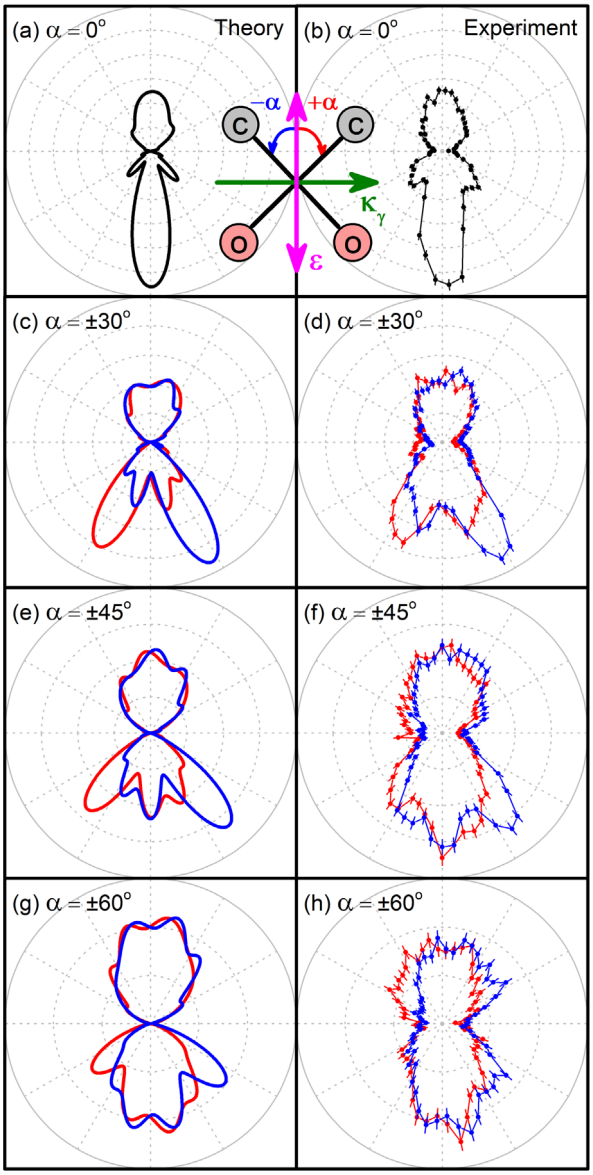


FIG. 3. Theoretical (left panels) and experimental (right panels) nondipole angular emission distribution of the C 1*s* photoelectrons of CO ionized by photons with an energy of 905 eV. The molecule is oriented as shown in the inset in the picture plane at an angle $\pm\alpha$ with respect to the polarization plane (magenta double arrow) of the circularly polarized ionizing light which propagates from left to right (green arrow).

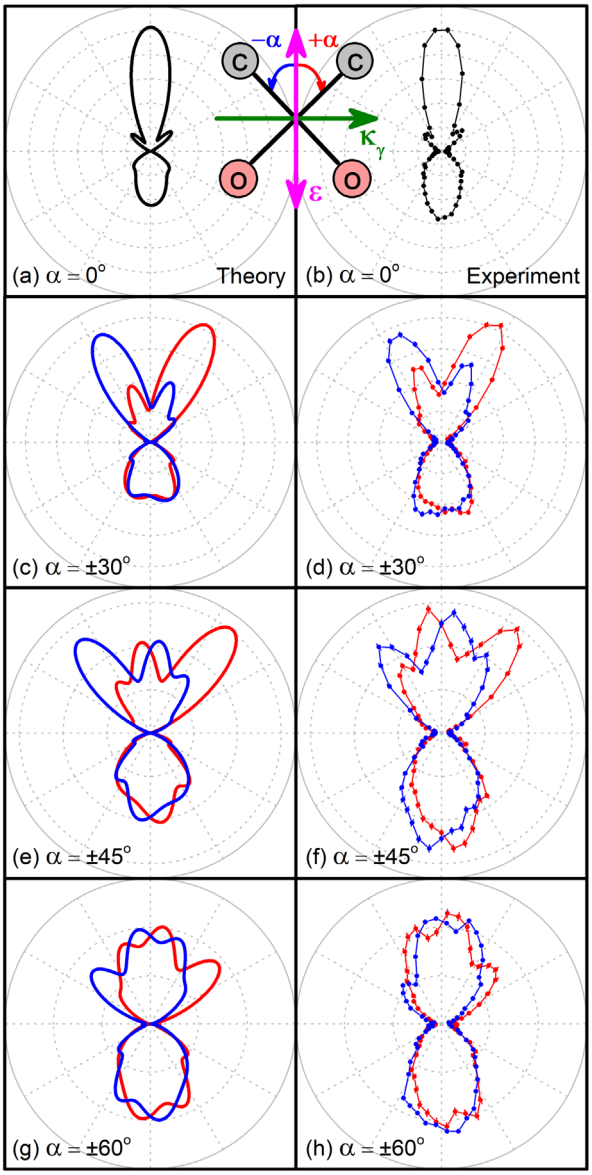


FIG. 4. Theoretical (left panels) and experimental (right panels) nondipole angular emission distribution of the O 1*s* photoelectrons of CO ionized by photons with an energy of 905 eV. The molecule is oriented as shown in the inset in the picture plane at an angle $\pm\alpha$ with respect to the polarization plane (magenta double arrow) of the circularly polarized ionizing light which propagates from left to right (green arrow).

orientation angle of $\alpha \pm 10°$. This uncertainty in the determination of the molecular orientation washes out some details of the experimental distributions as compared to the theory. Individual impacts of those averaging effects are visualized in Supplemental Material [38] with the help of the present theoretical data. Remaining disagreements might be attributed to limitations of the present theory, e.g., to the one-particle description of photoelectron waves in the frozen-core Hartree-Fock approximation.

As a final point, we demonstrate in Fig. 5 that this nondipole-induced asymmetry survives an averaging over the photoelectron emission directions. Such a total electron yield can be considered as a measure of the total ionization rate which, of course, depends on the molecular orientation (owing to the main lobe in the photoelectron angular emission distributions). However, in the dipole approximation, it should be equal for two $\pm\alpha$ mirrored orientations of the molecule with respect to the polarization plane. Solid black curves in Figs. 5(a) and 5(b) depict the presently computed total yields of the respective C and O 1*s* photoelectrons in the considered emission plane, and they exhibit a clear asymmetry [i.e., their maxima are slightly

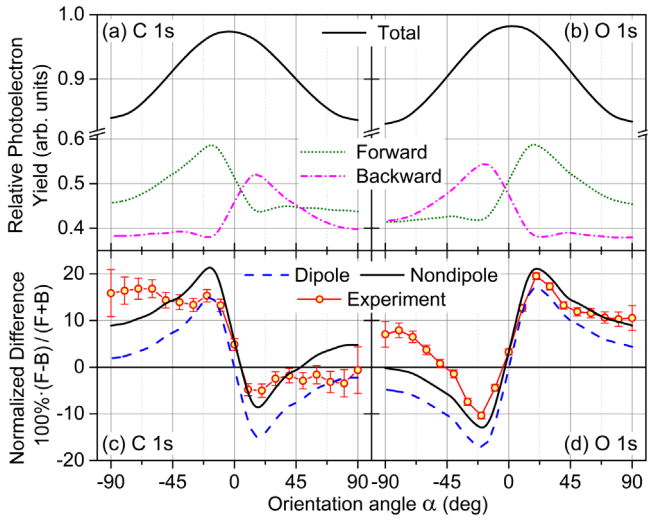


FIG. 5. (a) and (b) Relative yields of the C 1$s$ and O 1$s$ photoelectrons in the plane built by the molecular axis and the light propagation direction as functions of the molecular orientation angle with respect to the polarization plane, as computed with the full treatment of the nondipole effects, together with their breakup in the forward and backward hemiplanes (see the legends). (c) and (d) Normalized difference between the respective forward and backward yields, $100\%.\, 100\% \cdot (F-B)/(F+B)$, as computed in the dipole approximation and with the full treatment of the nondipole effects, together with the present experimental results (see the legend).

shifted to negative (positive) orientation angles for the carbon (oxygen) emitters]. Much higher contrast in the asymmetry can be seen if one considers the total photoemission yields in the forward and backward hemiplanes separately [broken curves in Figs. 5(a) and 5(b)].

Experimentally, this small asymmetry is beyond the systematical errors of our ion detector. To still test the underlying effect, we depict in Figs. 5(c) and 5(d) the normalized differences of these computed forward and backward electron yields (solid black curves). As one can see, they exhibit a clear oscillatory structure from positive to negative values for carbon and vise versa for oxygen emitters. However, the computed differences are not antisymmetric with respect to the polarization plane ($\alpha = 0°$) being clearly shifted to positive values (upward) as compared to those computed in the dipole approximation (dashed blue curves). The systematical error in these normalized differences is significantly smaller than in our measured absolute rates. As one can see, the respective experimental normalized differences (symbols with error bars as statistical uncertainties), which need not be calibrated for different orientation angles $|\alpha|$, fully support the theoretically demonstrated asymmetry. The measured normalized differences are, however, somewhat washed out by the discussed above uncertainties in the determination of the molecular orientation angle $\alpha$.

In conclusion, we observe an asymmetry in the angle-resolved photoemission from CO molecules oriented at two equal but mirrored angles with respect to the polarization plane of circularly polarized 905 eV synchrotron radiation. In the dipole approximation, the respective photoelectron emission distributions are perfect mirror images of each other. Owing to the retardation of short-wavelength ionizing radiation, the main lobe in the photoemission, which points toward the scatterer atom, is notably enhanced or reduced if the neighboring atom is oriented along the light propagation or in the opposite direction. The present Letter provides a showcase example for the manifestation of nondipole effects, which can be expected in future ultrafast photoelectron diffraction imaging experiments at high-photon-energy facilities.

This work was supported by the Deutsche Forschungsgemeinschaft (DFG): experiment within Project No. 447234583 (DO 604/38-1) and theory by Project No. 492619011 (DE 2366/6-1). We acknowledge DESY (Hamburg, Germany), a member of the Helmholtz Association HGF, for the provision of experimental facilities. This research were carried out at PETRA III within Proposal No. I-20190706, and we thank the staff of beam line P04 for excellent support during the beam time. This research was supported in part through the Maxwell computational resources operated at DESY.

*doerner@atom.uni-frankfurt.de
†demekhin@physik.uni-kassel.de

[1] B. Krässig, M. Jung, D. S. Gemmell, E. P. Kanter, T. LeBrun, S. H. Southworth, and L. Young, Phys. Rev. Lett. **75**, 4736 (1995).
[2] D. W. Lindle and O. Hemmers, J. Electron Spectrosc. Relat. Phenom. **100**, 297 (1999).
[3] R. W. Dunford, E. P. Kanter, B. Krässig, S. H. Southworth, and L. Young, Radiat. Phys. Chem. **70**, 149 (2004).
[4] K. Lin, S. Eckart, A. Hartung, D. Trabert, K. Fehre, J. Rist, L. Ph. H. Schmidt, M. S. Schöffler, T. Jahnke, M. Kunitski, and R. Dörner, Sci. Adv. **8**, 7386 (2022).
[5] C. T. L. Smeenk, L. Arissian, B. Zhou, A. Mysyrowicz, D. M. Villeneuve, A. Staudte, and P. B. Corkum, Phys. Rev. Lett. **106**, 193002 (2011).
[6] A. Ludwig, J. Maurer, B. W. Mayer, C. R. Phillips, L. Gallmann, and U. Keller, Phys. Rev. Lett. **113**, 243001 (2014).
[7] A. Hartung, S. Eckart, S. Brennecke, J. Rist, D. Trabert, K. Fehre, M. Richter, H. Sann, S. Zeller, K. Henrichs, G. Kastirke, J. Hoehl, A. Kalinin, M. S. Schöffler, T. Jahnke, L. Ph. H. Schmidt, M. Lein, M. Kunitski, and R. Dörner, Nat. Phys. **15**, 1222 (2019).
[8] K. Lin, S. Brennecke, H. Ni, X. Chen, A. Hartung, D. Trabert, K. Fehre, J. Rist, X.-M. Tong, J. Burgdörfer, L. Ph. H. Schmidt, M. S. Schöffler, T. Jahnke, M. Kunitski, F. He, M. Lein, S. Eckart, and R. Dörner, Phys. Rev. Lett. **128**, 023201 (2022).
[9] A. Hartung, S. Brennecke, K. Lin, D. Trabert, K. Fehre, J. Rist, M. S. Schöffler, T. Jahnke, L. Ph. H. Schmidt,

M. Kunitski, M. Lein, R. Dörner, and S. Eckart, Phys. Rev. Lett. **126**, 053202 (2021).
[10] S. Grundmann, M. Kircher, I. Vela-Peréz, G. Nalin, D. Trabert, N. Anders, N. Melzer, J. Rist, A. Pier, N. Strenger, J. Siebert, Ph. V. Demekhin, L. Ph. H. Schmidt, F. Trinter, M. S. Schöffler, T. Jahnke, and R. Dörner, Phys. Rev. Lett. **124**, 233201 (2020).
[11] S. Grundmann, D. Trabert, K. Fehre, N. Strenger, A. Pier, L. Kaiser, M. Kircher, M. Weller, S. Eckart, L. Ph. H. Schmidt, F. Trinter, T. Jahnke, M. S. Schöffler, and R. Dörner, Science **370**, 339 (2020).
[12] M. Ya. Amusia, E. G. Drukarev, V. G. Gorshkov, and M. O. Kazachkov, J. Phys. B **8**, 1248 (1975).
[13] M. S. Schöffler, C. Stuck, M. Waitz, F. Trinter, T. Jahnke, U. Lenz, M. Jones, A. Belkacem, A. L. Landers, M. S. Pindzola, C. L. Cocke, J. Colgan, A. Kheifets, I. Bray, H. Schmidt-Böcking, R. Dörner, and Th. Weber, Phys. Rev. Lett. **111**, 013003 (2013).
[14] S. Grundmann, F. Trinter, A. W. Bray, S. Eckart, J. Rist, G. Kastirke, D. Metz, S. Klumpp, J. Viefhaus, L. Ph. H. Schmidt, J. B. Williams, R. Dörner, T. Jahnke, M. S. Schöffler, and A. S. Kheifets, Phys. Rev. Lett. **121**, 173003 (2018).
[15] E. Shigemasa, J. Adachi, K. Soejima, N. Watanabe, A. Yagishita, and N. A. Cherepkov, Phys. Rev. Lett. **80**, 1622 (1998).
[16] J. G. Underwood and K. L. Reid, J. Chem. Phys. **113**, 1067 (2000).
[17] A. Landers, Th. Weber, I. Ali, A. Cassimi, M. Hattass, O. Jagutzki, A. Nauert, T. Osipov, A. Staudte, M. H. Prior, H. Schmidt-Böcking, C. L. Cocke, and R. Dörner, Phys. Rev. Lett. **87**, 013002 (2001).
[18] R. Guillemin, O. Hemmers, D. W. Lindle, E. Shigemasa, K. Le Guen, D. Ceolin, C. Miron, N. Leclercq, P. Morin, M. Simon, and P. W. Langhoff, Phys. Rev. Lett. **89**, 033002 (2002).
[19] R. Guillemin, E. Shigemasa, K. Le Guen, D. Ceolin, C. Miron, N. Leclercq, K. Ueda, P. Morin, and M. Simon, Rev. Sci. Instrum. **71**, 4387 (2000).
[20] M. Simon, M. N. Piancastelli, and D. W. Lindle, Hard-X-ray Photoelectron Spectroscopy of Atoms and Molecules, in *Hard X-ray Photoelectron Spectroscopy (HAXPES)*, edited by J. Woicik (Springer International Publishing, New York, 2016), pp. 65–110.
[21] A. N. Grum-Grzhimailo, J. Phys. B **36**, 2385 (2003).
[22] Ph. V. Demekhin, A. Ehresmann, and V. L. Sukhorukov, J. Chem. Phys. **134**, 024113 (2011).
[23] Ph. V. Demekhin, D. V. Omel'yanenko, B. M. Lagutin, V. L. Sukhorukov, L. Werner, A. Ehresmann, K.-H. Schartner, and H. Schmoranzer, Opt. Spectrosc. **102**, 318 (2007).
[24] N. M. Novikovskiy, A. N. Artemyev, D. V. Rezvan, B. M. Lagutin, and Ph. V. Demekhin, J. Phys. B **55**, 175001 (2022).
[25] K. P. Huber and G. Herzberg, *Molecular Spectra and Molecular Structure. IV. Constants of Diatomic Molecules* (Springer, New York, NY, 1979).
[26] M. W. Schmidt, K. K. Baldrige, J. A. Boatz, S. T. Elbert, M. S. Gordon, J. H. Jensen, S. Koseki, N. Matsunaga, K. A. Nguyen, S. Su, T. L. Windus, M. Dupuis, and J. A. Montgomery, Jr., J. Comput. Chem. **14**, 1347 (1993).
[27] T. H. Dunning, Jr., J. Chem. Phys. **55**, 716 (1971).
[28] M. Kircher, J. Rist, F. Trinter, S. Grundmann, M. Waitz, N. Melzer, I. Vela-Peréz, T. Mletzko, A. Pier, N. Strenger, J. Siebert, R. Janssen, L. Ph. H. Schmidt, A. N. Artemyev, M. S. Schöffler, T. Jahnke, R. Dörner, and Ph. V. Demekhin, Phys. Rev. Lett. **123**, 243201 (2019).
[29] L. Kaiser, K. Fehre, N. M. Novikovskiy, J. Stindl, D. Tsitsonis, G. Gopakumar, I. Unger, J. Söderström, O. Björneholm, M. Schöffler, T. Jahnke, R. Dörner, F. Trinter, and Ph. V. Demekhin, J. Phys. B **53**, 194002 (2020).
[30] I. Vela-Peréz *et al.*, arXiv:2105.11897.
[31] J. Viefhaus, F. Scholz, S. Deinert, L. Glaser, M. Ilchen, J. Seltmann, P. Walter, and F. Siewert, Nucl. Instrum. Methods Phys. Res., Sect. A **710**, 151 (2013).
[32] R. Dörner, V. Mergel, O. Jagutzki, L. Spielberger, J. Ullrich, R. Moshammer, and H. Schmidt-Böcking, Phys. Rep. **330**, 95 (2000).
[33] J. Ullrich, R. Moshammer, A. Dorn, R. Dörner, L. Ph. H. Schmidt, and H. Schmidt-Böcking, Rep. Prog. Phys. **66**, 1463 (2003).
[34] T. Jahnke, Th. Weber, T. Osipov, A. L. Landers, O. Jagutzki, L. Ph. H. Schmidt, C. L. Cocke, M. H. Prior, H. Schmidt-Böcking, and R. Dörner, J. Electron Spectrosc. Relat. Phenom. **141**, 229 (2004).
[35] O. Jagutzki, V. Mergel, K. Ullmann-Pfleger, L. Spielberger, U. Spillmann, R. Dörner, and H. Schmidt-Böcking, Nucl. Instrum. Methods Phys. Res., Sect. A **477**, 244 (2002).
[36] O. Jagutzki, J. S. Lapington, L. B. C. Worth, U. Spillman, V. Mergel, and H. Schmidt-Böcking, Nucl. Instrum. Methods Phys. Res., Sect. A **477**, 256 (2002).
[37] R. N. Zare, Mol. Photochem. **4**, 1 (1972).
[38] See Supplemental Material at http://link.aps.org/supplemental/10.1103/PhysRevLett.129.253201 which contains Fig. S1 for individual impacts of different averaging effects.